Journal of Membrane Science 455 (2014) 162–167

Contents lists available at ScienceDirect

Journal of Membrane Science

journal homepage: www.elsevier.com/locate/memsci

Flux of silver-carbonate membranes for post-combustion CO_2 capture: The effects of membrane thickness, gas concentration and time

Lingling Zhang [a], Yunhui Gong [a], Kyle S. Brinkman [b], Tao Wei [a], Siwei Wang [a], Kevin Huang [a,*]

[a] Department of Mechanical Engineering, University of South Carolina, Columbia, SC 29208, United States
[b] Science and Technology Directorate, Savannah River National Laboratory, Aiken, SC 29808, United States

ARTICLE INFO

Article history:
Received 13 November 2013
Received in revised form
15 December 2013
Accepted 29 December 2013
Available online 7 January 2014

Keywords:
CO_2 separation
Critical thickness
CO_2 concentration
Surface-modification
Stability

ABSTRACT

In this paper, we systematically studied the effects of membrane thickness, CO_2 concentration, and operating time on the CO_2 flux density of an Al_2O_3-surface-modified and carbon-black-pore-former derived silver-carbonate membrane. It was found that the CO_2 transport through a silver-carbonate membrane exhibited a critical thickness of 0.84 mm, below which no flux enhancement could be achieved. The CO_2 flux was also observed to be proportional to the difference of ($P_{CO_2}P_{O_2}^{1/2}$) at the two reacting surfaces, and not the commonly assumed logarithmic partial pressure difference. The CO_2 flux tested against time at 650 °C increased by 200% for the first 160 h, followed by a gradual decrease. At the 326-h marker, the flux was still the same as the original value when the test was started. Overall, the use of carbon black as a pore-former and Al_2O_3 as a surface modifier for silver-carbonate membranes has been proven effective and necessary to achieve a higher and more stable CO_2 flux density.

1. Introduction

Capture of post-combusted CO_2 from predominant fossil-fueled power plants is of technological importance to the stabilization of atmospheric CO_2 concentration and mitigation of global warming and climate change. The conventional solvent and sorbent based CO_2 capture technologies are costly, cumbersome and energy intensive [1–4]. With the existing material systems and engineering designs, it seems difficult to overcome the grand challenges in cost and energy penalty for years to come. Development of new, cost-effective and energy-efficient CO_2 capture technologies is, therefore, imperative.

Recently, we demonstrated high-flux silver-carbonate mixed electron and carbonate-ion conducting (MECC) membranes suitable for post-combustion CO_2 capture. This new class of electrochemical membranes in theory can exclusively and continuously separate CO_2 from a CO_2 source such as flue gas at high temperatures [5–7]. The working principle of the membrane is based on a concomitant migration of CO_3^{2-} and e^- under a chemical gradient of CO_2 and O_2 across the membrane, thus transporting CO_2 and O_2 from higher concentration to capture side. The captured CO_2–O_2 has been suggested to convert into a mixture of easily separable CO_2 and H_2O mixture by combusting in a syngas. The large amount of heat can be recovered to produce steam for electricity [8]. It has also been suggested to recycle back to the combustion chamber for oxy-combustion. Therefore, MECC membrane has great potential to play an important role in stabilizing the atmospheric CO_2 concentration by capturing CO_2 emitted from the existing fossil-fueled power plants. Since the capture process is continuous and operated at elevated temperatures, the new membranes have great potential to be a cost-effective and energy-efficient CO_2 capture technology. We also showed that the long-term stability of the membrane can be significantly improved by modifying the surface of porous silver networks with a thin layer of Al_2O_3 [9].

In previous study, the microcrystalline methylcellulose has been used as a pore-former to fabricate the porous silver matrix. Based on the knowledge we have learned from mixed oxide-ion and carbonate-ion conductor (MOCC), smaller pore size and uniform porous structure are among keys to achieving high CO_2 flux density [10–13]. In this study, we further expand the previous study by investigating the effects of membrane thickness, CO_2 concentration and time on the flux of CO_2 permeation. While the same Al_2O_3 surface modification on silver network was kept for the present work, a new pore-former carbon black, which is one of the widely used pore-former [14,15], was tested with a goal to create a better connected porous silver network.

2. Experimental procedure

2.1. Synthesis of silver-carbonate membranes

A two-step approach was employed to synthesize the dual-phase silver-carbonate MECC membranes. The porous silver

* Corresponding author. Tel.: +1 803 777 0204.
E-mail address: kevin.huang@sc.edu (K. Huang).

0376-7388/$ - see front matter © 2014 Elsevier B.V. All rights reserved.
http://dx.doi.org/10.1016/j.memsci.2013.12.077

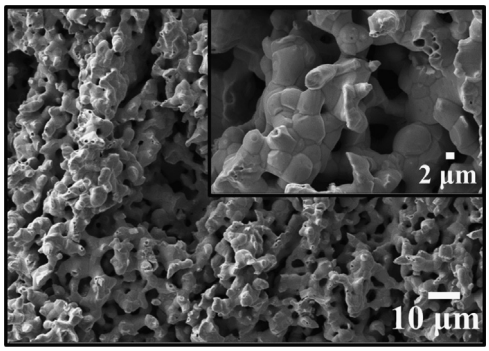

Fig. 1. The cross-sectional view of microstructure of a porous Ag matrix created by carbon black as a pore former.

matrix was first fabricated by intimately mixing silver powders (99.9%, Alfa Asear) with carbon black as a pore-former (Alfa Asear) in a ratio of 60:40 (vol%). The powder was ball-milled (Mix/Mill 8000M, Spex Sample Prep) and uniaxially pressed at 200 MPa into pellets using a static mold presser (18 mm in diameter), followed by firing at 650 °C for 2 h. After that, the sample was loaded into the vacuum impregnation unit (CitoVac, Struers). An Al_2O_3 colloidal solution (0.05 μm, Alfa Asear) with 5 wt% concentrations was then infiltrated into the porous silver scaffold for one time under a vacuum condition. After drying and firing at 400 °C for 2 h, the coated silver membrane was immerged into a carbonate melt containing a eutectic mixture of Li_2CO_3 (≥ 99%, Alfa Asear) and K_2CO_3 (≥ 99%, Alfa Asear) in 62:38 (mol%). The detail about this procedure can be found in our previous work [10,16–18].

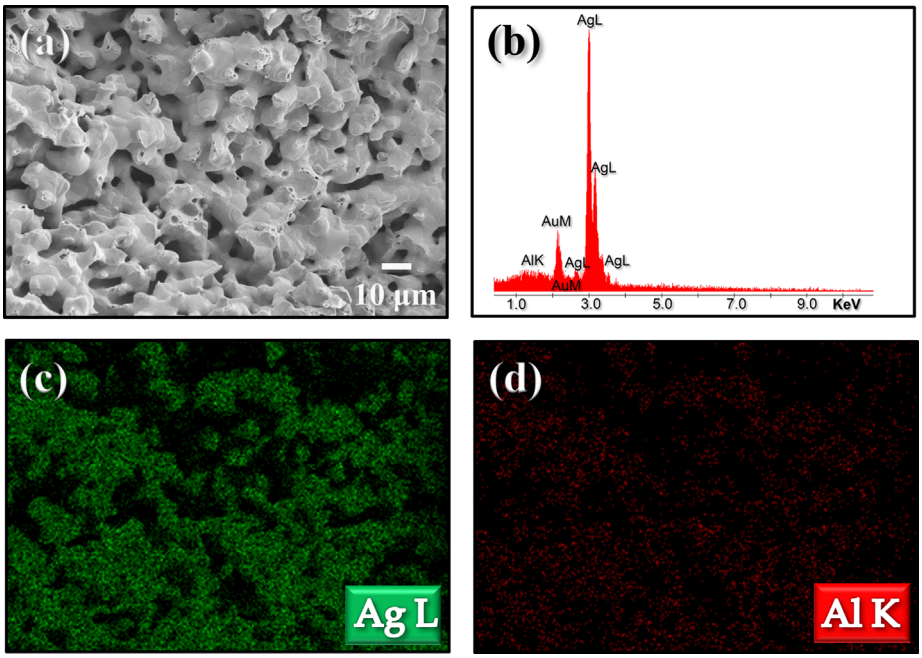

Fig. 2. (a) Microstructure and (b) EDS compositions of a porous Ag matrix coated with 5% Al_2O_3 colloidal; elemental distributions of Ag matrix with 5% Al_2O_3 colloidal (c) Ag mapping and (d) Al mapping.

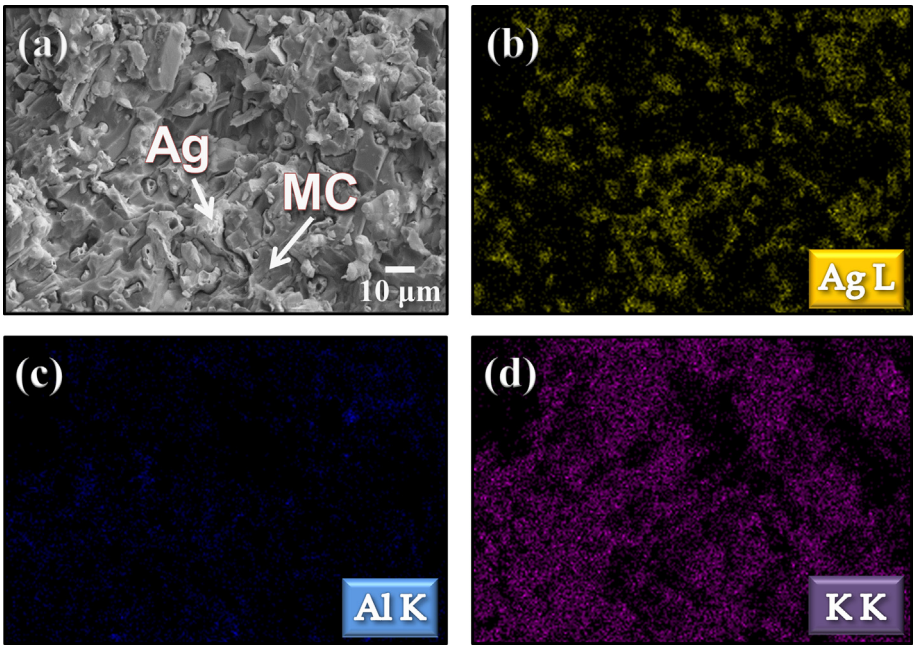

Fig. 3. Microstructure and elemental distributions of silver-carbonate MECC membrane decorated with Al_2O_3 coating (5% colloidal) before testing (a) SEM image; (b) Ag mapping; (c) Al mapping; and (d) K mapping. *Note*: Li is not detectable by EDS.

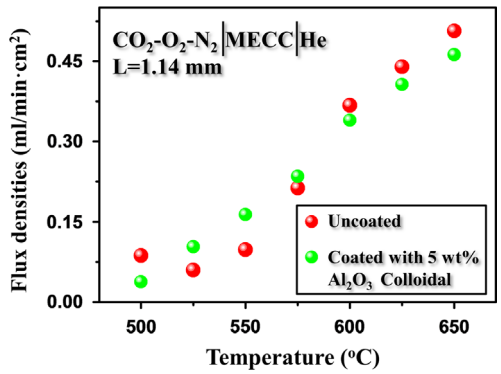

Fig. 4. CO_2 flux densities of uncoated and Al_2O_3-coated silver-carbonate membranes as a function of temperature.

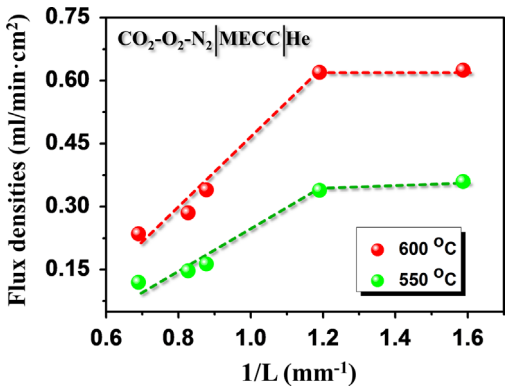

Fig. 5. CO_2 densities of MECC membrane as a function of the reciprocal of thickness at 550 °C and 600 °C.

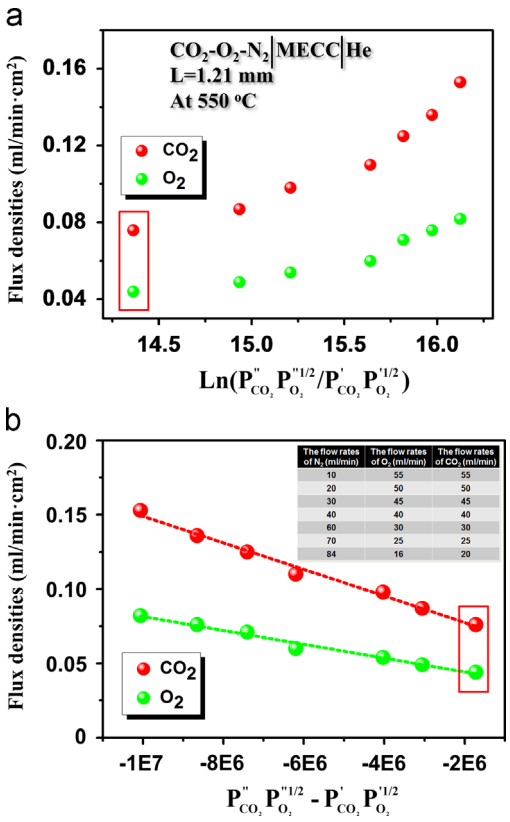

Fig. 6. CO_2 and O_2 flux densities of MECC membrane with the thickness of 1.21 mm as a function of CO_2 and O_2 chemical gradient at 550 °C; (a) with natural logarithmic relationship; (b) with a linear relationship of ($P_{CO_2}P_{O_2}^{1/2}$). Inset table: The actual flow rates of N_2, O_2 and CO_2 used for the test. The boxed data points represent the practical flue-gas composition of post-combustion.

The fabricated membrane was finally polished using ethyl alcohol as a solvent to remove the residual molten carbonate (MC) on the surfaces, followed by a gas tightness check using a homemade leak-check device before it was assembled into a permeation cell. The effective area of the membrane was 0.92 cm^2.

2.2. CO_2 flux measurement

The configurations of CO_2 permeation cell used in this study have been previously described [9,10]. The button-type membrane was first sealed to a supporting alumina tube with a commercial silver paste as a sealant. A second short alumina tube was then bonded to the top of the sample for the purpose of shielding the feed gas. The feed gas for regular study was a mixture of 50 ml min^{-1} O_2, 50 ml min^{-1} CO_2 and 20 ml min^{-1} N_2; N_2 was used as a tracer gas for leak correction if present. For the study of CO_2 concentration effects on flux density, the flow rates of CO_2 and O_2 were systematically varied in the range of 16–55 and 20–55 ml min^{-1}, respectively, while keeping their ratio as 1:1. The flow rate of N_2 was changed accordingly to keep the total gas flow ($CO_2+O_2+N_2$) rate at 120 ml min^{-1}. The actual flow rates of CO_2, O_2 and N_2 used for the study are shown in the inset table of Fig. 6(b). We particularly studied the effect of the actual flue gas composition emitted from a typical power plant; they are represented by the last row of flow rates and boxed data points. A high-purity helium (99.999%) at a flow rate of 50 ml min^{-1} was used as the sweeping gas, the composition of which was analyzed by an on-line micro-GC (Varian 490-GC, Varian). To ensure the accuracy, the GC was calibrated with four standard gas compositions for each gas of interest (CO_2, O_2, and N_2). The final CO_2 flux density was calculated out from an average gas composition of a total of ten successive readings from the GC. For all gas flows, commercial mass flow controllers (Smart-Trak, 50 Series) specifically calibrated for the gas under use were employed to control the mass flow rates. The temperature of permeation cells was varied from 500 to 650 °C in an interval of 25 °C. At each temperature, 30 min were given to allow the cell to reach steady state before sampling.

2.3. Other characterization

The microstructural features and elemental distributions of the porous silver matrix as well as MC-filled MECC membrane before and after long-term test were captured and analyzed by a field emission scanning electron microscopy (FESEM, Zeiss Ultra) equipped with energy dispersive X-ray spectroscopy (EDS) analyzer.

3. A modified CO_2 permeation flux equation for MECC membranes

3.1. Bulk-diffusion controlled transport

For bulk-diffusion controlled charge transport in homogeneous mixed conductors, the flux density J_i of the active species i is given by

$$J_i = -\frac{D_i C_i}{RT}\nabla\eta_i = -\frac{\sigma_i}{(z_i F)^2}\nabla\eta_i = -\frac{\sigma_i}{(z_i F)^2}(\nabla\mu_i + z_i F\nabla\phi) \quad (1)$$

where D_i, C_i, σ_i and z_i represent the self-diffusivity, concentration, conductivity and charge of species i, respectively; η_i and μ_i are electrochemical and chemical potentials of species i; R, F and T have their usual meanings. For a dual-phase MECC membrane, by setting

$1=CO_3^{2-}$ and $2=e^-$ Eq. (1) changes to

$$J_1 = -\frac{\sigma_1\sigma_2}{z_1^2F^2}\left(\frac{\nabla\mu_1 - z_1/z_2\nabla\mu_2}{\sigma_1+\sigma_2}\right) \quad (2)$$

Considering the local chemical equilibrium $CO_2+1/2O_2+2e^- = CO_3^{2-}$, one has

$$J_1 = J_{CO_3^{2-}} = -\frac{3}{8F^2}\left(\frac{\sigma_{CO_3^{2-}}\sigma_{e^-}}{\sigma_{CO_3^{2-}}+\sigma_{e^-}}\right)\left(\nabla \ln P_{CO_2} + \frac{1}{2}\nabla \ln P_{O_2}\right) \quad (3)$$

Assuming that $\sigma_{CO_3^{2-}}$ and σ_{e^-} are both P_{CO_2} and P_{O_2} independent, the steady-state flux $J_{CO_2}=J_{CO_3^{2-}}$ can be obtained by integrating across the thickness L of the membrane exposed to a gradient of high P'_{CO_2}, P'_{O_2} and low P''_{CO_2}, P''_{O_2}, leading to

$$J_{CO_2} = J_{CO_3^{2-}} = -\frac{3RT}{8F^2}\left(\frac{\sigma_{CO_3^{2-}}\sigma_{e^-}}{\sigma_{CO_3^{2-}}+\sigma_{e^-}}\right)\ln\frac{P''_{CO_2}, P''^{1/2}_{O_2}}{P'_{CO_2}, P'^{1/2}_{O_2}} \quad (4)$$

Considering the microstructural and volumetric effects, the final CO_2 flux density for MECC membranes is changed to

$$J_{CO_2} = -\left(\frac{\varepsilon}{\tau}\right)\frac{3RT}{8F^2L}\frac{\varphi\sigma_{CO_3^{2-}}(1-\varphi)\sigma_{e^-}}{\varphi\sigma_{CO_3^{2-}}+(1-\varphi)\sigma_{e^-}}\ln\frac{P''_{CO_2}, P''^{1/2}_{O_2}}{P'_{CO_2}, P'^{1/2}_{O_2}} \quad (5)$$

where ε and τ are the porosity and the tortuosity of the porous silver matrix, respectively; L is the thickness of the membrane, cm; φ is the volume fraction of the MC phase; $\sigma_{CO_3^{2-}}$ and σ_{e^-} are the conductivities of carbonate-ions and electrons in S/cm, respectively; P'_{CO_2}, P'_{O_2} and P''_{CO_2}, P''_{O_2} are the partial pressures of CO_2 and O_2 at the feed and permeate sides in Pa, respectively. Eq. (5) suggests that a plot of J_{CO_2} against logarithmic chemical gradient at a fixed temperature yields a straight-line.

3.2. Surface controlled transport

As the membrane thickness decreases, surface exchange kinetics becomes rate limiting, a characteristic of which is the critical thickness, L_c, represented by [19]

$$L_c = \frac{2D_{CO_3^{2-}}}{k_{CO_3^{2-}}} \quad (6)$$

where $D_{CO_3^{2-}}$ (cm^2/s) and $k_{CO_3^{2-}}$ (cm/s) are diffusivity and exchange coefficient of CO_3^{2-}, respectively. This ratio of the mobile ion's ability to diffuse compared to the rate of dissociation at the surface is vastly different depending on the nature of the ionic species. Smaller molecules such as hydrogen that have fast diffusivity but larger surface exchange rates exhibit L_c in the range of 1 μm [20]. In comparison, the L_c of most oxygen ion transport membranes is two orders of magnitude higher in the range of 100 μm [19]. There is little existing experimental data in the literature on the thickness dependence of flux for metal-carbonate dual-phase membranes.

Considering the surface-exchange limitation to the overall CO_2 flux density, the thickness L in the bulk-diffusion controlled flux equations such as Eqs. (4) and (5) becomes the effective thickness L_e

$$L_e = \frac{1}{1+(2L_c/L)}L \quad (7)$$

It is evident that the flux of CO_2 across the membrane is reduced by a factor of $1/(1+2L_c/L)$.

4. Results and discussion

4.1. Microstructural features

The cross sectional view of microstructure from a porous silver matrix made with carbon black as a pore-former is shown in Fig. 1. It is evident that the matrix exhibits a rather uniformly distributed porous structure with the pore size ~10 μm. Compared to porous silver network created by microcrystalline methylcellulose pore former which is 15–20 μm in size as previously reported [9], carbon black derived pores are smaller and more uniform. The microstructures of a porous silver matrix coated with an Al_2O_3 layer is shown in Fig. 2(a). The homogenous porous structure was not affected by the Al_2O_3 coating, but its pore size was decreased to ~8 μm. The EDS analysis shown in Fig. 2(b)–(d) confirms the presence as well as uniform distribution of Al_2O_3 in the matrix. The dense microstructure of the final as-synthesized carbonate-filled silver network (MECC) is evidently shown in Fig. 3(a). The compositional EDS analysis shown in Fig. 3(b)–(d) also suggests a uniform distribution of Ag, Al_2O_3 and MC phases across the membrane.

4.2. The effect of Al_2O_3 coating on CO_2 flux

The CO_2 flux densities measured from silver-carbonate membrane (denoted as Sample-A) and the one coated with 5 wt% Al_2O_3 colloidal (denoted as Sample-B) are shown in Fig. 4 as a function of temperatures. As expected, the CO_2 flux densities increase with temperature, confirming that the transport of CO_3^{2-} and e^- is a thermally activated process. Compared to silver-carbonate membrane with microcrystalline methylcellulose as pore-former, carbon black derived membranes exhibit roughly 1.5 times higher flux density [9]. On the other hand, the flux densities of the uncoated and coated samples are equivalent over the temperature range tested, which suggests that the 5 wt% colloidal Al_2O_3 coated layer does not significantly affect the transport of CO_3^{2-}. This finding is consistent with our previous study, which was also concluded that this composition yielded a more stable flux than the uncoated samples [9]. Therefore, silver-carbonate membrane coated with 5 wt% Al_2O_3 colloidal was used as a standard for studying the effects of membrane thickness and CO_2 concentration.

4.3. The effect of membrane thickness on CO_2 flux density

The effect of membrane's thickness (L) on CO_2 flux density was investigated with five levels of thicknesses: 0.63, 0.84, 1.14, 1.21 and 1.45 mm. The CO_2 density as a function of the $1/L$ at 550 °C and 600 °C are shown in Fig. 5. It is evident that the CO_2 flux densities exhibit almost a linear relationship with $1/L$ when L ranges from 0.84 to 1.45 mm, but a plateau at $L<0.84$ mm. According to Eq. (5), the linear relationship between J_{CO_2} and $1/L$ at $L\geq 0.84$ mm suggests a bulk-diffusion controlled CO_2 transport mechanism. Below 0.84 mm, the insensitivity of J_{CO_2} to $1/L$ implies that surface exchange kinetics involving CO_2 and O_2 begins to dominate the overall CO_2 flux, which is a thickness-independent process. Therefore, the critical thickness of CO_2 transport through silver-carbonate membranes is $L_c=0.84$ mm. From Fig. 5, it is also interesting to note that L_c is insensitive to temperature within 550–600 °C, implying that the surface exchange and bulk diffusion may have a similar activation energy. A silver-carbonate membrane with $L<0.84$ mm would not further promote CO_2 permeation flux.

The significantly greater L_c than those for H_2 and O_2 permeation membranes is not surprising due to the size, complexity and anticipated slow surface-exchange rate of the CO_3^{2-} compared to simpler O^{2-} and H^+ ionic species. Higher L_c value implies easy domination of surface-exchange kinetics in CO_2 transport in metal-carbonate dual-phase membranes. The ceramic-carbonate

CO_2 membranes have also exhibited deviation from the linear $J_{CO_2} \sim 1/L$ relationship. In this case, a 10-μm thick YSZ-carbonate membrane exhibited a flux of only 10 times larger than that for the 200-μm thick samples compared to a 30 fold increase if the behavior followed the linear relation [21]. More surface analysis is needed to further clarify the adsorption and desorption mechanisms in the future.

4.4. The effect of CO_2 concentration on CO_2 flux

The dependence of CO_2 and O_2 flux densities of the silver-carbonate membrane on CO_2 concentration is shown in Fig. 6. In the bulk-diffusion controlled flux equation (Eq. (5)), the conductivity of CO_3^{2-} ($\sigma_{CO_3^{2-}}$) is assumed to be independent of P_{CO_2} and P_{O_2}. The resultant J_{CO_2} should, therefore, be proportional to $\ln(P_{CO_2}P_{O_2}^{1/2})$. However, such a relationship is not supported by the experimental data shown in Fig. 6(a). This discrepancy implies the assumption that $\sigma_{CO_3^{2-}}$ is independent of P_{CO_2} and P_{O_2} is problematic. According to the basic surface reaction $CO_2 + 1/2O_2 + 2e^- = CO_3^{2-}$, it would seem to be reasonable to assume that the concentration of CO_3^{2-} and therefore $\sigma_{CO_3^{2-}}$ has the following dependence of P_{CO_2} and P_{O_2}:

$$\sigma_{CO_3^{2-}} = \sigma^o P_{CO_2} P_{O_2}^{1/2} \quad (8)$$

where σ^o is a constant. Substituting Eq. (8) into Eq. (3) and integrating over the range of chemical gradients of CO_2 and O_2 and thickness with the assumption of $\sigma_{CO_3^{2-}} \ll \sigma_{e^-}$ yield the following new flux equation:

$$J_{CO_2} = -\left(\frac{\varepsilon}{\tau}\right)\frac{3RT}{8F^2L}\varphi\sigma^o(P''_{CO_2}P''^{1/2}_{O_2} - P'_{CO_2}P'^{1/2}_{O_2}) \quad (9)$$

It is evident from this equation that J_{CO_2} is proportional to the difference of $(P_{CO_2}P_{O_2}^{1/2})$ at the two reacting surfaces. Following this new flux equation, we re-plot the J_{CO_2} in Fig. 6(b) and find a nearly perfect linear relationship between the two. This finding suggests that Eq. (8) is an adequate expression to describe the dependence of $\sigma_{CO_3^{2-}}$ on P_{CO_2} and P_{O_2}. On the other hand, it is also interesting to note that the CO_2 flux under a practical flue gas composition (boxed data point in Fig. 6) can be as high as 0.08 ml min^{-1} cm^{-2} at 550 °C.

4.5. Long-term testing

The long-term variability of CO_2, O_2 and N_2 flux densities is shown in Fig. 7. The membrane exhibits CO_2 and O_2 flux densities of 0.28 and 0.145 ml cm^{-2} min^{-1}, respectively, at the beginning. The flux densities keep increasing with time during the first 160 h, reaching 0.60 and 0.32 ml cm^{-2} min^{-1} in approximately 2:1 ratio. This represents a 200% increase in CO_2 flux density from the beginning. After 160 h, the flux begins to gradually decrease. At the 326-h marker, the CO_2 and O_2 flux densities reach 0.26 and 0.13 ml cm^{-2} min^{-1}, still in 2:1 ratio, roughly the same as the original values.

To further understand the enhancement and degradation mechanisms, SEM/EDS analysis were conducted. The elemental distributions of the upstream side of silver-carbonate membrane constituents are shown in Fig. 8, which suggests that Ag, Al_2O_3 and MC phases are still well distributed across the membrane even after the long-term test. There is no obvious change in phase compositions and microstructure from the original sample. By comparing the morphologies of the pre- (Fig. 3) and post-test

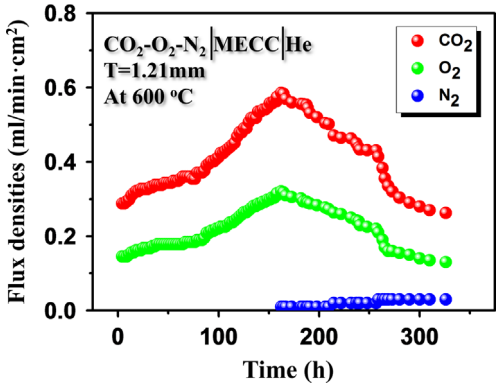

Fig. 7. Long-term flux variability of CO_2, O_2 and N_2 of MECC membrane evaluated at 600 °C.

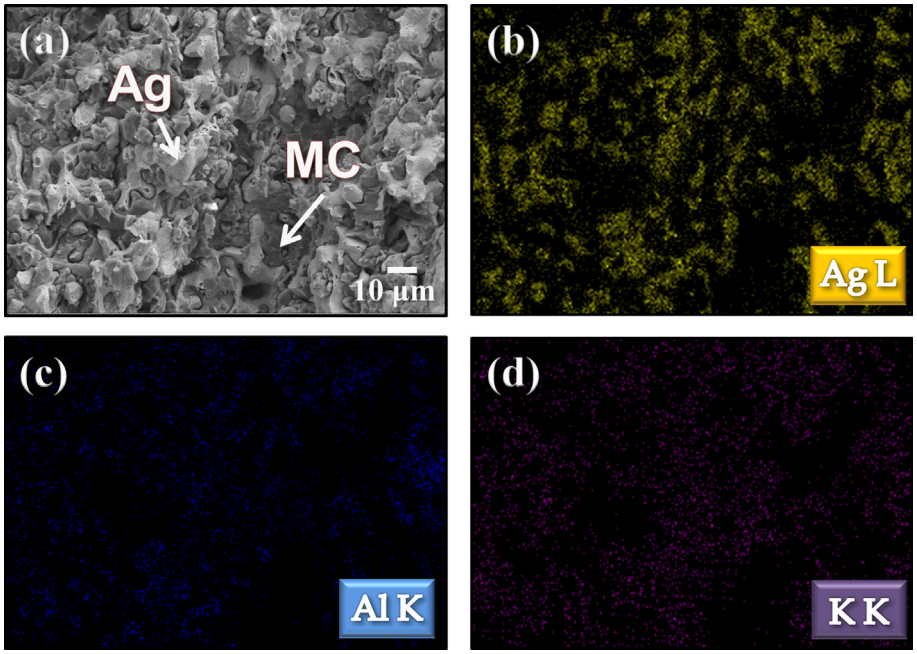

Fig. 8. Microstructure and elemental distributions of Sample-B after a long-term flux variability test (a) SEM image; (b) Ag mapping; (c) Al mapping; and (d) K mapping. *Note*: Li is not detectable by EDS.

samples, it seems to suggest that loss of the MC in the membrane has occurred during the test. This finding can be related to the increase in flux shown in Fig. 7 in the sense that effective thickness of the membrane has been reduced due to a loss of MC. As the loss of MC continues and accumulates, the integrity of the membrane was eventually compromised at the end of testing as indicated by the increase in the concentration of tracer gas N_2 in the sweeping He. The 160-h marker appeared to be the tipping point as a result of the MC-loss process.

5. Conclusions

Using carbon black as a pore former and Al_2O_3 as a surface modifier, silver-carbonate membranes have been demonstrated with the CO_2 flux density that follows a linear relationship with $1/L$ at $L \geq 0.84$ mm, suggesting a bulk-diffusion controlling mechanism. Below 0.84 mm, the flux remains flat, suggesting that the rate-limiting step has shifted to the concurrent surface exchange kinetics of CO_2 and O_2. The CO_2 flux density has also been found proportional to the difference of $(P_{CO_2}P_{O_2}^{1/2})$ at the two reacting surfaces, not the commonly assumed logarithmic pressure difference, implying that the conductivity of CO_3^{2-} in the mixed conducting membrane is dependent on P_{CO_2} and P_{O_2}. For a long-term test at 650 °C, the CO_2 flux density was observed to increase by 200% for the first 160 h, following by a gradual decrease for the next 160 h. At the 326-h marker, the flux was still the same as the original value. Overall, uses of carbon black as a pore former and Al_2O_3 as a surface modifier for silver-carbonate membranes are proven effective and necessary to achieve a higher and more stable CO_2 flux density.

Acknowledgments

Financial support from NSF (CBET-1340269, CBET-124706) and the U.S. Army Research Laboratory and the U.S. Army Research Office (W911NF-10-R-006) are greatly appreciated.

Nomenclature

i	charge species
J_i	flux density
D_i	self-diffusivity
C_i	concentration
σ_i	conductivity
R	gas constant
F	Faraday constant
T	temperature
L	thickness
P'_{CO_2}	partial press of CO_2 at the feed side
P''_{CO_2}	partial press of CO_2 at the permeate side
P'_{O_2}	partial press of O_2 at the feed side
P''_{O_2}	partial press of O_2 at the permeate side
ε	porosity
τ	tortuosity
φ	volume fraction of the MC phase
k_i	surface exchange coefficient
L_c	critical thickness

References

[1] C. Stewart, M.A. Hessami, A study of methods of carbon dioxide capture and sequestration––the sustainability of a photosynthetic bioreactor approach, Energy Conver. Manage. 46 (3) (2005) 403–420.
[2] ARPA-E Carbon Capture Programs, Taillores Post-Combustion Carbon Capture Workshop, July 11, 2010.
[3] C.F. Hendricks, Carbon dioxide removal from coal-fired power plants, Energy Environ. 1 (1994) 19–49.
[4] D. Shekhawal, D.R. Luebke, H.W. Pennline, A Review of Carbon Dioxide Selective Membranes, National Energy Technology Laboratory, DOE/NETL, 2003.
[5] S.J. Chung, J.H. Park, D. Li, J.-I. Ida, I. Kumakiri, Y.S. Lin, Dual-phase metal-carbonate membrane for high-temperature carbon dioxide separation, Ind. Eng. Chem. Res. 44 (2005) 7999–8006.
[6] N. Xu, X. Li, M.A. Franks, H. Zhao, K. Huang, Silver-molten carbonate composite as a new high-flux membrane for electrochemical separation of CO_2 from flue gas, J. Membr. Sci. 401–402 (2012) 190–194.
[7] L. Bastin, P.S. Brcia, E.J. Hurtado, J.A.C. Silva, A.E. Rodrigues, B. Chen, A microporous metal-organic framework for separation of CO_2/N_2 and CO_2/CH_4 by fixed-bed adsorption, J. Phys. Chem. C 112 (5) (2008) 1575–1581.
[8] S.R. Sherman, J.R. Gray, K.S. Brinkman, K. Huang, Combustion-assisted CO_2 capture using MECC membranes, J. Membr. Sci. 401–402 (2012) 323–332.
[9] L. Zhang, Y. Gong, J. Yaggie, S. Wang, K. Romito, K. Huang, Surface modified silver-carbonate mixed conducting membranes for high flux CO_2 separation with enhanced stability, J. Membr. Sci. 453 (2014) 36–41.
[10] L. Zhang, N. Xu, X. Li, S. Wang, K. Huang, W.H. Harris, W.K.S. Chiu, High CO_2 permeation flux enabled by highly interconnected three-dimensional ionic channels in selective CO_2 separation membranes, Energy Environ. Sci. 5 (2012) 8310–8317.
[11] M. Anderson, Y.S. Lin, Carbonate–ceramic dual-phase membrane for carbon dioxide separation, J. Membr. Sci. 357 (2010) 122–129.
[12] Z. Rui, M. Anderson, Y. Li, Y.S. Lin, Ionic conducting ceramic and carbonate dual phase membranes for carbon dioxide separation, J. Membr. Sci. 174 (2012) 417–418.
[13] J. Ortiz-Landeros, T.T. Norton, Y.S. Lin, Effects of support pore structure on carbon dioxide permeation of ceramiccarbonate dual-phase membranes, Chem. Eng. Sci. 104 (2013) 891–898.
[14] A. Sanson, P. Pinasco, E. Roncari, Influence of pore formers on slurry composition and microstructure of tape casting supporting anodes for SOFCs, J. Eur. Ceram. Soc. 6 (2008) 1221–1226.
[15] L. Nie, J. Liu, Y. Zhang, M. Liu, Effects of pore formers on microstructure and performance of cathode membranes for solid oxide fuel cells, J. Power Sources 196 (2011) 9975–9979.
[16] L. Zhang, X. Huang, C. Qin, K. Brinkman, Y. Gong, S. Wang, K. Huang, First spectroscopic identification of pyrocarbonate for high CO_2 flux membranes containing highly interconnected three dimensional ionic channels, Phys. Chem. Chem. Phys. 15 (2013) 13147–13152.
[17] L. Zhang, X. Li, S. Wang, K.G. Romito, K. Huang, High conductivity mixed oxide-ion and carbonate-ion conductors supported by a prefabricated porous solid-oxide matrix, Electrochem. Commun. 13 (2011) 554–557.
[18] L. Zhang, Z. Mao, J.D. Thomason, S. Wang, K. Huang, Synthesis of a homogeneously porous solid oxide matrix with tunable porosity and pore size, J. Am. Ceram. Soc. 95 (2012) 1832–1837.
[19] H.J.M. Bouwmeester, H. Kruidhof, A.J. Burggraaf, Importance of the surface exchange kinetics as rate-limiting step in oxygen permeation through mixed-conducting oxides, Solid State Ion. 72 (1994) 185–194.
[20] S.N. Paglieri, J.D. Way, Innovations in palladium membrane research, Sep. Purif. Methods 31 (2002) 1–169.
[21] B. Lu, Y.S. Lin, Synthesis and characterization of thin ceramic-carbonate dual-phase membranes for carbon dioxide separation, J. Membr. Sci. 444 (2013) 402–411.